UNIVERSITAT DE BARCELONA

FACULTAT DE FÍSICA

Master in Biophysics

Rheology of complex fluids
Stochastic switches in the galactose signalling network

Final project of Master in Biophysics 2007/08:
Laura Casanellas Vilageliu

Tutors: Jordi Ortín - Marta Ibañes

The present work is formed by two different projects, both included in the biophysics area. The first one is experimental and studies the rheology of complex fluids. The second one, theoretical and numerical, deals with stochastic switches in systems exhibiting bistability. Having started one of them, I had the opportunity to begin an experimental PhD, and considering the two subjects really amazing I decided to keep working, and do the final project of the Master in Biophysics on both of them.

Contents

Part I
Rheology of complex fluids

Abstract

Many biological fluids are complex fluids. Complex fluids present a particular mesoscopic structure which provides them viscoelastic effects, among others. These fluids can show viscous or solid behavior depending on the time-scale in which they are operating. These properties can have a major influence on the biological processes in which the fluids are involved. Rheological techniques can be applied in order to characterize these fluids. In the present work experiments using a cone-plane geometry rheometer will be done on a complex fluid with worm-like chain micellar structure, CPyCl-NaSal [100:60], in order to present a complete rheological characterization. In addition, a particular example of biorheology applied to blood samples will be presented.

1 Introduction

A wide classification can be done of different liquids found in nature. On one hand, Newtonian fluids, which have been extensively described and understood throughout physics's history. Some important candidates are water or oil. Their Newtonian behavior is mainly characterized by a constant viscosity under an applied shear stress and a hydrodinamic flow given by the Navier-Stokes equations. On the other hand, the so called Non-Newtonian fluids, in comparison to the Newtonian ones, which have unusual properties. Non-Newtonian fluids can have variable viscosity, normal forces or viscoelastic properties which are all translated into a wide range of observed bizarre phenomena (Weissenberg, die swell or tubeless siphon effects, see fig 1).

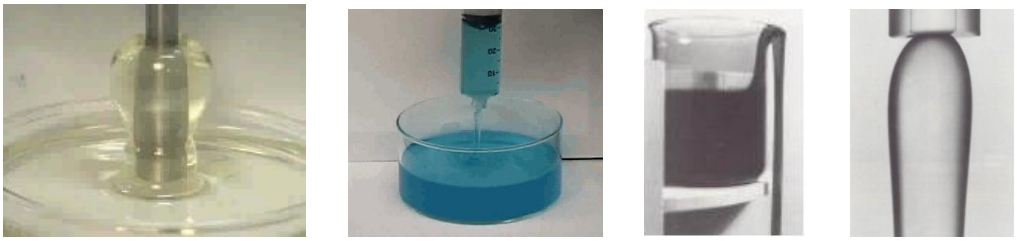

Figure 1: a. Weissenberg or *rod climbing* effect: the fluid which is placed in a container with a central rod is submitted to an external rotation. The fluid tends to climb, unexpectedly, toward the central rod; b.c. *Siphon effect*: the fluid is dragged out of the container without an external force; d. *Die swell*: the fluid blows up when it exits an open end of a die. Adapted from the Rheological laboratory of Toronto website.

All these amazing properties have important technological applications in pharmaceutical or food industry but they also play a crucial role in the scientific area.

Non-newtonian effects are directly related to complex fluids. Complex fluids are fluids which are disordered in the microscopic length scale ($\sim \mathring{A}$), structured in the mesoscopic

(∼nm) and homogeneous in the macroscopic one (∼mm). Some examples of complex fluids are polymeric solutions (or biopolymeric), surfactant solutions (microemulsions or micellar solutions) and colloidal suspensions (ink, milk, foams or emulsions). Their inner mesoscopic structure is responsible for their particular non-Newtonian behavior.

When complex fluids are submitted to external perturbations like hydrodynamic fluxes they may respond, in comparison to Newtonian fluids, like a solid and a liquid at the same time (they are *viscoelastic*). Solid like behavior is related to the elasticity of the material and liquid like to the viscous and dissipative.

The hydrodynamics of viscoelastic fluids is still not completely well known and constitutes an area of current research in fluid physics. It has recently been discovered that viscoelastic fluids loose their stability under external perturbations to become weakly turbulent at low Reynolds numbers, which is never possible in Newtonian fluids where turbulence always appears due to inertial terms at high Reynolds numbers.

A way to extract information of the fluid flow is by means of rheological experiments. Macroscopic rheology studies the fluid behavior under applied shear or extensional stresses in specific geometric conditions.

In the present work we start describing accurately the properties of complex fluids and in particular of complex fluids found in living beings, that we call complex *biofluids* (Chap. 2). Later on, a theoretical approach to complex fluids is presented (Chap. 3) paying special attention to the linear Maxwell model. The aim of the experimental part (Chap. 4) is to prove the theoretical model with experimental data taken on a micellar solution prepared in the laboratory, and do a complete rheological characterization of this fluid. Finally, a study of blood samples is presented (Chap. 5).

2 Complex fluids

2.1 Generalities

A key feature of complex fluids is the dependence of their viscosity on an externally applied shear stress, which is equivalent to a non linear relation between the applied shear stress and the resulting rate of deformation of the fluid. In Newtonian fluids the situation is much simpler: the viscosity is constant and the relation is linear. Many different behaviors are observed. On one hand, there exist the so called shear thinning fluids (or pseudoplastic fluids). Their viscosity decreases as the rate of deformation is increased. These fluids can be formed by particles or droplets of different shapes dispersed in a liquid or by polymer solutions of long entangled chains. At zero shear stress molecules are distributed in a random way, due to the Browmian motion. When an external shear stress is applied particles start to deform and align in the direction of the applied stress and polymer chains disentangle leading to a decrease of the viscosity (fig. 2). Consequently, the fluid flows more easily. This property has important implications in pharmaceutical and chemical industry but also in biology (Sec. 2.3). If eventually the shear stress is removed, the polymeric structure can be recovered and particles come to their original shape after some characteristic time.

On the other hand, shear thickening fluids (also called dilatant) increase their vis-

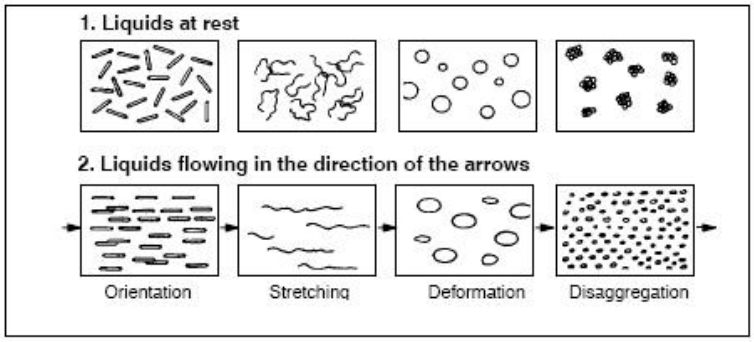

Figure 2: Dispersions at rest and flowing through a tube [1]

cosity when a shear rate is applied. They are much less abundant than shear-thinning ones.

Some fluids have a yield stress value and they do not flow if applied shear stresses are smaller, or they are thixotropic and their viscosity is time dependent.

However, viscoelasticity is maybe the non-newtonian effect of main interest in complex fluids. As we have mentioned viscoelastic fluids have an intermediate behavior between solids and fluids. Polymeric solutions with large elastic molecules and long relaxation processes are generally sensitive to exhibit viscoelastic effects. It depends, anyway, on the concentration of polymers and on their length. For small concentrations the fluid is mainly viscous (and the fluid only dissipates energy). As the concentration increases polymers start to overlap, forming a mesh (semi dilute regime), and viscoelastic effects start to be relevant (energy dissipation and energy storage coexist). At a certain concentration (the entanglement concentration), polymers start to reptate between them leading to an entangled rheology which modifies drastically the viscoelasticity. Viscoelastic properties will be specially studied in the course of the present work.

2.2 Approximations at different length scales

In order to understand the reason why complex fluids present viscoelastic and other non-Newtonian effects we should look into their molecular structure. Theoretical microscopic approximations based on statistical mechanics of macromolecules (in polymeric solutions they mainly consider their reptation and self-assembly modes in entangled regimes [2]) have been developed.

However, there also exist macroscopic empirical approximations of complex fluids which do not consider their molecular structure but reveal its macroscopic behavior (we could call them *black box* models). Their constitutive equation (that relates the applied stress to the resulting shear rate of the fluid) contains an elastic part and a viscous or dissipative one, which are modeled by elastic springs and dashpots, respectively. The main advantage of these models is that they are simpler than the microscopic ones and easier to deal with. In addition, they are in good agreement with experimental data [3].

2.3 Complex biofluids

Many complex fluids are present in living beings. Their non-Newtonian properties are associated to the function they have to perform. In many biological processes, like blood cells pumped through arteries, the way how energy is dissipated or stored is of key importance and this is given by the viscoelasticity of the material. In an analogous way non-Newtonian effects play a key role in processes where synovial fluid is involved. The synovial fluid is localized in synovial joints and is needed to reduce the friction between cartilage and the surrounding tissue. Hyaluronic acid contained in that fluid provides him rheological properties that give mobility to the joint [4]. Synovial fluid is shear-thinning and that adds advantageous properties to its lubricating function (when an applied shear rate is increased the viscosity and the resistive force decrease).

Complex biofluids can be found in biopolymeric solutions (neutral or charged), physical gels or colloidal dispersions. Some examples of neutral polymeric solutions are intermediate filaments, actin, peptide fibrils or microtubules of eukaryotic cells [4]. Nucleic acid constitutes another interesting example of polymeric (charged) solution. It has important rheological applications because it can be used to analyze results of electrophoresis experiments and, due to its large size, it allows to do rheological experiments of single molecules too.

Physical gels are networks formed by an ensemble of polymeric components cross-linked by weak *physical* bounds (in comparison to chemical) such as electrostatic or hydrogen bonds and surrounded by a solvent. Starches or pectins are some current exam-ples. The cytoskeleton of eukaryotic cells is formed by an active gel of actin filaments. Active gels are very similar to *passive* gels. The main difference is the ability that active gels have to generate, by means of ATP consumption, a net stress inside the gel that tends to contract the cell.

Rheological properties of biocolloidal dispersions may vary with the colloid concentration, volume fraction or the externally applied shear rate. Globular proteins solutions (blood as the most relevant one) as well as icosahedral viruses solutions are some examples of important complex fluids with biological interest.

3 Macroscopic rheology

Rheology studies the flow of a fluid under any externally applied stress. It allows to analyze different fluid properties for different shear stress regimes and it is useful to determine if a fluid is Newtonian or not and identify which non-Newtonian phenomena presents. Rheometers are the experimental setup used to do these experiments. Two main different types of rheological experiments can be done: shear flow, in which a shear stress is applied (fig. 3), or extensional experiments with an applied extensional stress. In this work it will be sufficient to deal only with shear flow rheology.

3.1 Shear-flow

Shear-flow experiments are the most used in rheological measurements. All shear flow experiments are based on the same essential idea. We will focus on the plate-plate

geometry which is the simplest one to obtain the theoretical expressions (fig. 3).

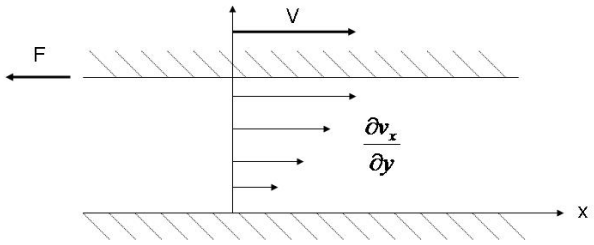

Figure 3: Shear flow in a plate-plate geometry. An external velocity V is applied to the upper plate while the lower one is at rest. A frictional force F appears as a response to the relative motion of both plates.

In shear flow experiments an external shear strain rate is applied and the fluid responds with a shear stress (or viceversa). The stress tensor, which is defined as the force per unit area, contains an isotropic and an anisotropic part. In a tensorial notation it is given by,

$$\sigma_{ij} = \tau_{ij} - p\delta_{ij} \; . \tag{1}$$

The isotropic one corresponds to the hydrostatic pressure and when the fluid is at rest it is the only non-vanishing one. The anisotropic one (τ), which we will call, for convenience and from now on, stress tensor itself, is responsible for the fluid flow [3]. In a plate-plate geometry the upper plate is moving in x-direction at a constant velocity V externally imposed, while the lower one is at rest, so that a velocity gradient is originated in the y-vertical direction.

In Newtonian fluids the stress tensor can be related to the shear rate by a linear relation given by the viscosity (η),

$$\tau = -\eta\dot{\gamma} \tag{2}$$

where $\dot{\gamma} = \frac{1}{2}\left(\frac{\partial v_i}{\partial x_j} + \frac{\partial v_j}{\partial x_i}\right)$. The only non-vanishing term for that particular geometry is τ_{xy} (and τ_{yx} because of the stress tensor's symmetry). Equation (2) is the constitutive equation for this fluid. The constitutive equation gives the relation between the stress tensor (τ) and the shear rate of deformation ($\dot{\gamma}$) for any fluid and it is the basic equation characterizing the fluid properties.

The constitutive equation for a viscoelastic fluid given the same geometry is

$$\sigma = \tau - p\delta = \begin{pmatrix} \tau_{xx} - p & \tau_{xy} & 0 \\ \tau_{yx} & \tau_{yy} - p & 0 \\ 0 & 0 & \tau_{zz} - p \end{pmatrix} \quad . \tag{3}$$

An essential difference between viscoelastic and Newtonian fluids is the existence of normal stresses (τ_{xx}, τ_{yy}, τ_{zz}) in the diagonal terms of the matrix that act perpendicular to the applied shear stress.

Differences between normal forces are used to determine the fluid behavior and can be measured experimentally:

$$N_1 = \tau_{xx} - \tau_{yy},$$
$$N_2 = \tau_{yy} - \tau_{zz}\ . \tag{4}$$

In Newtonian fluids normal stress differences are always equal to zero.

The second difference N_2 is generally much smaller than the first one N_1 and it is neglected (in addition it is hard to measure experimentally). Normal stresses give amazing properties to the fluid. For example, they are responsible for the *rod-climbing* and *die swell* effects (see fig 1).

Like in Newtonian fluids, in viscoelastic fluids the tangential shear stress is related to the viscous behavior of the fluid. Equation (4), equivalent to equation (2) for Newtonian fluids, gives the relation between τ and $\dot{\gamma}$, but in this case the viscosity is not constant.

$$\tau_{xy} = -\eta\left(\dot{\gamma}\right)\dot{\gamma} \tag{5}$$

3.2 Models of viscoelastic fluids. Maxwell model

The aim of any non-Newtonian fluid model is to find the constitutive equation describing its behavior. The constitutive equation for the linear Maxwell model is [2]:

$$\tau + t_m \frac{\partial \tau}{\partial t} = -\eta_0 \dot{\gamma}\ , \tag{6}$$

where,

$$t_m = \frac{\eta_0}{G_0} \tag{7}$$

is the characteristic and unique relaxation time of the fluid. It represents a characteristic time scale because it distinguishes both elastic and viscous behaviors. For times shorter than t_m the fluid is mainly viscous and for longer times the elastic behavior dominates:

$$t \gg t_m \rightarrow \tau + \underbrace{t_m \frac{\partial \tau}{\partial t}}_{0} = -\eta_0 \dot{\gamma} \rightarrow \tau = -\eta_0 \dot{\gamma} \rightarrow \text{ viscous behavior.} \tag{8}$$

$$t \ll t_m \rightarrow \underbrace{\frac{\tau}{t_m}}_{0} + \frac{\partial \tau}{\partial t} = -G_0 \dot{\gamma} \rightarrow \tau = -G_0 \gamma \rightarrow \text{ elastic behavior.} \tag{9}$$

The linear Maxwell model is a macroscopic approximation that models the fluid with one elastic spring and one dissipative dashpot connected in series. There also exist other models, more complex, that describe more accurately the fluid, such as the UCM (upper-convected Model), that ensures that equations of motion are Galilean invariant, or the Oldroyd-B model. But they go beyond the scope of the present work.

Fluids following the linear Maxwell model do not really exist in nature. However, the model is well accomplished for many fluids in low shear rate regimes [2]. Micellar fluids fit particularly well with this model.

Different rheological experiments can be performed to measure transient properties of viscoelastic fluids and prove if those fluids behave as Maxwell fluids (Chap.4).

3.3 Other complex fluids

It is worth to comment that there are also fluids that have the same constitutive equation as the Newtonian fluids (they do not present normal forces) but are not Newtonian. It is because their viscosity depends on the applied shear rate. Pseudoplastic and dilatant fluids (Chap. 2) do present this behavior. The relation between the effective viscosity and the shear rate can be described by a power law relation [8],

$$\eta = K \cdot \gamma^{-m} \tag{10}$$

where the exponent m can be determined experimentally.

4 Experimental rheology

4.1 Experimental setup

The fluid we will use in order to do the rheological characterization is a solution made of Cetylpyridinium chloride (CPyCl) and Sodium Salicylate (NaSal) diluted in distilled water in a concentration $[100 : 60]$ mM. The solution has been prepared in the labo-

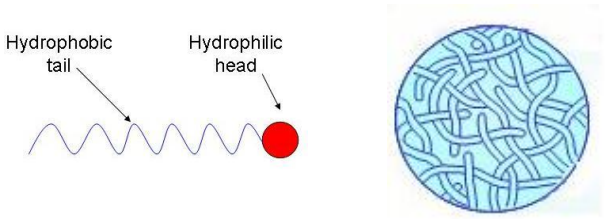

Figure 4: Left: Amphiphilic surfactant molecule. Right: Entangled regime of wormlike micelles.

ratory by adding weighted amounts of the two salts to double-distilled water, shaking it vigorously, and let in a dark chamber for four days approximately before using it to let the entrained air to leave. This fluid is formed by amphiphilic molecules (with an hydrophilic head and an hydrophobic tail) that tend to rearrange forming micelles (fig. 4). We are working with a concentration of surfactant above the critical micellar concentration (CMC) that gives entangled cylindrical (or wormlike) flexible micelles [2] (fig. 4).

We are most interested in this fluid because it is well known that it behaves as a perfect Maxwellian fluid in low shear regimes [5, 6]. Rheological properties depend on thermodynamic variables like surfactant concentration or temperature. For simplicity we will keep them constant throughout all the work. The temperature of the experiments will be $T = 25$ ° C in every case.

A rheometer Haake RheoStress1 is used to do the rheological measurements. It has a cone-plate geometry with an outer diameter of 60 mm and an angle (α) of 1° (fig. 5). The cone is truncated in order to avoid any wear between the tip and the plate. The

main advantage of this geometry is that the shear rate of deformation ($\dot{\gamma}$) is constant on any point of the cone surface.

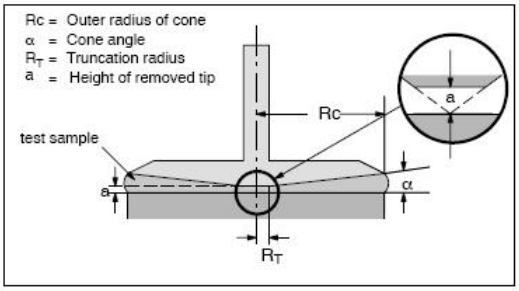

Figure 5: Cone-plate system [1].

The rheometer can operate in two different modes:

- CS: a controlled external shear stress is applied to the sample and the resulting shear rate is measured.
- CR: a controlled external shear rate is applied and the resulting shear stress is measured.

Depending on every specific measurement one mode will be more suitable than the other one.

4.2 Results

4.2.1 Linear viscoelastic regime

Different rheological tests can be used to obtain information about the rheological properties of the fluid. To get this information it is necessary that the fluid structure is preserved while experiments are running. Oscillatory tests are the most frequently used for that purpose. In order to preserve linear viscoelasticity small amplitudes and low shear rates have to be applied.

In oscillatory experiments a sinusoidal shear stress is applied and the resulting deformation, or rate of deformation, is measured.

The oscillatory stress is given by

$$\tau^*(t) = \tau_0 \exp\left(i(\omega t + \phi)\right) \ , \tag{11}$$

and the resulting deformation of the fluid,

$$\gamma^*(t) = \gamma_0 \exp\left(i\omega t\right) \ . \tag{12}$$

They are related by the complex modulus G^*:

$$\tau^*(t) = G^*(w)\gamma^*(t) = \left(G'(\omega) + iG''(\omega)\right)\gamma^*(t) \ . \tag{13}$$

$G'(\omega)$ is the *elastic modulus*, which is related to the elastic behavior, and $G''(\omega)$ is the *loss modulus* and it is related to the viscous one. Depending on the fluid-solid prevalence $\tau^*(t)$ and $\gamma^*(t)$ will be in phase, $\delta = 0°$, (elastic behavior) or out of phase, $\delta = 90°$, (dissipative behavior). The phase will be given by

$$\frac{G''(\omega)}{G'(\omega)} = \frac{G^* \sin\delta}{G^* \cos\delta} = \tan\delta\,, \tag{14}$$

and measuring it we can predict which behavior dominates at each frequency. For a perfect solid $G'(\omega) = G_0$ and $G''(\omega) = 0$, and for a Newtonian fluid $G'(\omega) = 0$ and $G''(\omega) = \eta\omega$.

In Maxwell fluids G' and G'' have the following specific expressions [5]

$$G'(\omega) = \frac{G_0 \omega^2 {t_m}^2}{(1+\omega^2 {t_m}^2)}\,, \tag{15}$$

$$G''(\omega) = \frac{G_0 \omega t_m}{(1+\omega^2 {t_m}^2)}\,, \tag{16}$$

and $t_m = \eta_0/G_0$ is the characteristic relaxation Maxwell time.

To find the suitable linear range preliminary experiments have to be done. In the linear viscoelastic regime viscoelastic functions such as the *loss* and the *storage modulus* remain constant under the applied stress. Measuring these functions versus the applied stress we can easily determine the linear stress regime as the region where they are constant. This procedure must be repeated for all the frequencies of interest. According to fig. 6, we select $\tau = 1$ Pa to be a suitable stress value.

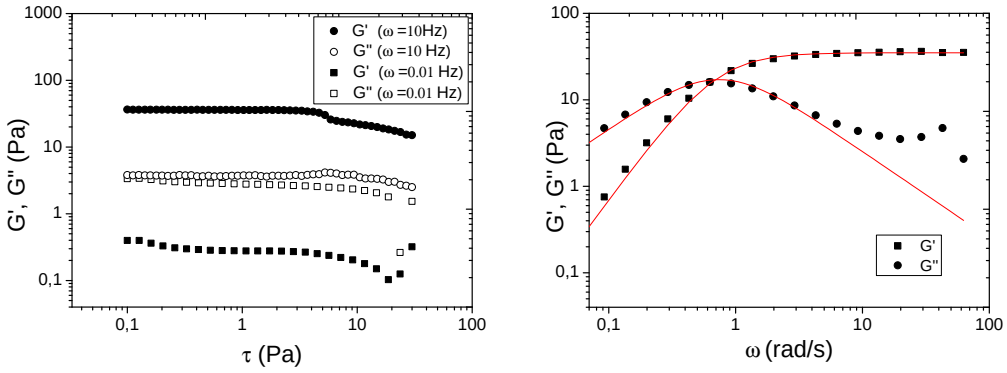

Figure 6: Left: Storage modulus (G') and loss modulus (G'') versus applied shear stress for a CPyCl-NaSal [100 : 60] mM solution at $T = 25°$ C. Right: Storage and loss moduli versus angular frequency for a CPyCl-NaSal [100 : 60] solution at $T = 25°$ C. Experimental results (dots) and analytical fitting curves (solid lines).

In fig. 6 experimental data and analytical fit, taken from Eqs (15) and (16) of G' and G'', are plotted. We can appreciate, as expected, that they match better for low shear regimes. We could extract rheological parameters (G_0 and t_m) from those fits. However it is preferable to find the intersection of both viscoelastic functions G' and G''. This point corresponds to $\omega = 1/t_m$. The obtained value for the characteristic relaxation time is $t_m = 1.6$ s, which is in good agreement with the literature [5, 6, 7].

In addition, the evolution of t_m in time has been measured (fig. 7). The characteristic relaxation time has been systematically determined every day for a period of 15 days. For the first 8 days t_m varies considerably but it tends to reach an almost constant value beyond the 10th day, approximately (which is the value we will use).

Another test can be done to verify if the fluid behaves as a Maxwellian fluid. It is the so called Cole-Cole plot, which represents G'' versus G'. From equations (15) and (16) we realise that this relation follows the equation of a circle of radius $G_0/2$ centered at $(0, G_0/2)$:

$$(G'(w) - \frac{G_0}{2})^2 + (G''(w))^2 = \left(\frac{G_0}{2}\right)^2 . \tag{17}$$

We can appreciate a good agreement between our experimental data and the analytical fit (fig. 7). The derived value of the shear modulus is $G_0 = 34.7 \pm 0.4$ Pa which is, again, in good agreement with the literature [6, 7].

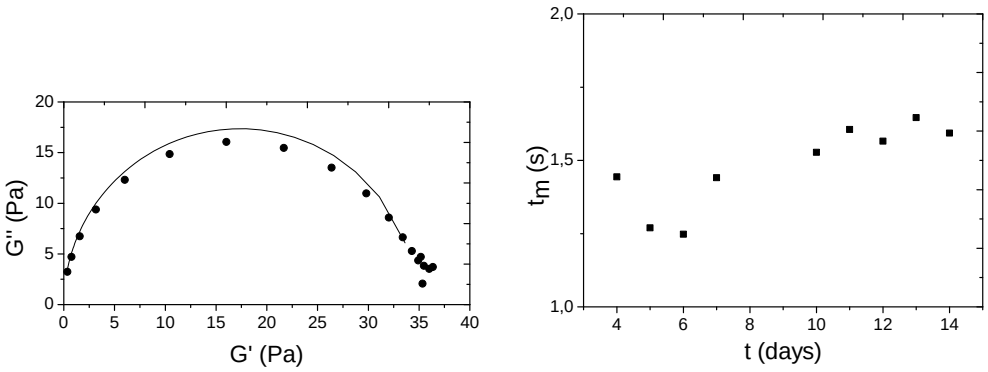

Figure 7: Left: Loss modulus (G'') versus storage modulus (G') for a CPyCl-NaSal [100 : 60] mM solution at $T = 25°$C. Right: Time evolution of a CPyCl-NaSal [100 : 60] mM solution at $T = 25°$C for a period of 14 days.

4.2.2 Non-linear regime

In non-linear regime the inner structure of the fluid is damaged. The applied stress is no longer proportional to the shear rate and the viscosity is not constant. In that regime rotatory tests are performed. A shear stress (or shear rate) is applied and the resulting shear rate (or shear stress) is measured. In figs. 8 and 9 we can easily distinguish the linear regime from the non-linear one which is strongly shear-thinning (for $\dot{\gamma} > 0.6\,\mathrm{s}^{-1}$).

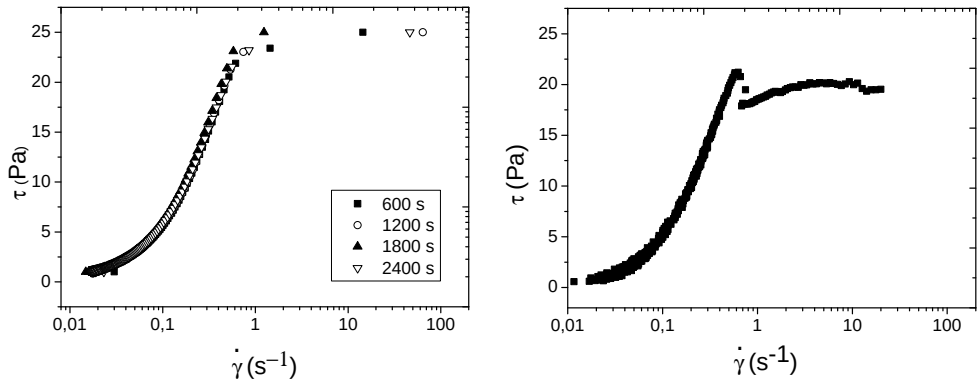

Figure 8: Shear stress versus shear rate for a CPyCl-NaSal [100 : 60] mM solution at T =25° C: Left: controlled stress mode (CS) for ramps of different duration; Right: controlled rate mode (CR).

Controlled stress and controlled rate experiments have been done. In CS the stress has been increased logarithmically from 1 Pa to 25 Pa in ramps of different time duration (fig. 8). In CR the shear strain has been increased logarithmically from 0.01 s^{-1} to 20 s^{-1} (fig. 8). It is important to realise that in the linear regime the resulting curve does not depend on the performed test. However in the non-linear regime it does. For different ramp durations in CS mode we can already notice little variations. But an enormous difference exists between CS and CR mode. In CR the stress smoothly increases to reach a maximum value ($\simeq$ 21 Pa at $\dot{\gamma} = 0.6$ s^{-1}) and suddenly decreases to a nearly constant value between $19 - 20$ Pa. This difference is due to the history dependence of the sample at this regime.

Finally, if we plot the shear viscosity versus the applied shear stress (measured in the CS mode) we can, again, easily visualize the shear-thinning behavior of the CPyCl solution (fig. 9). According to equation (10) describing the shear-thinning behavior of a fluid we can extract, from the non-linear regime, the fit parameters $K = 23.9 \pm 0.5$ Pa, $m = 0.85 \pm 0.03$, and roughly approximating them we obtain the resulting power law expression

$$\eta \approx 24\,\dot{\gamma}^{-1}\,. \tag{18}$$

In addition we can extrapolate from fig. 9 the zero-shear viscosity ($\dot{\gamma} \to 0$) to be

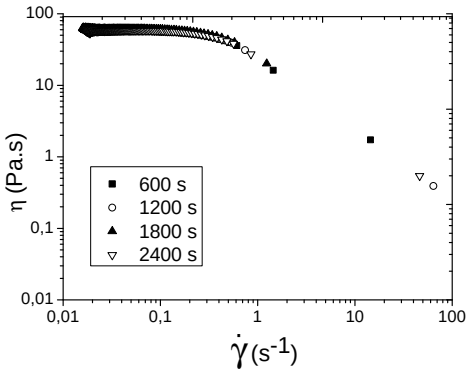

Figure 9: Shear viscosity versus shear rate for a CPyCl-NaSal [100 : 60] mM solution at $T = 25°C$. Controlled stress mode (CS) and ramps of different duration.

$\eta_0 = 60$ Pa·s, which is in fair agreement with Eq. (7), ($\eta_0 = G_0 \cdot t_m$), for the results we have obtained.

4.2.3 Normal stress differences

A Haake Mars Rheometer has been used to measure normal stress differences. It has the same geometry and operational modes as the Rheostress1 we have been using until now with the additional capacity of measuring normal forces.

A shear stress experiment in CR mode (with $0 < \dot{\gamma} < 200$ s^{-1}) has been done.

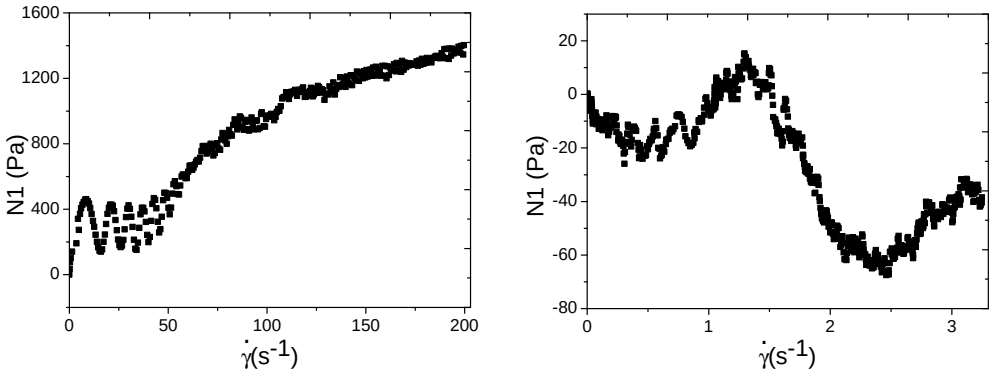

Figure 10: First normal stress differences (N1) versus applied shear rate, for a CPyCl-NaSal [100 : 60] mM solution at $T = 25°C$.

Important oscillations in normal stress differences ($N1$) are observed in the range $0 \leq \dot{\gamma} < 50\ \mathrm{s}^{-1}$ (fig. 10) with a later increase to very large values of $N1$. Another experiment focusing on low shear rate values has been performed to verify if oscillations also existed in low shear rate regimes. It has been successfully verified as we can appreciate in fig. 10.

These oscillations are associated in the literature to shear-banding. The fluid would separate in two phases with different effective viscosity, one supporting higher values of shear stresses than the other one [9, 10].

5 Rheology of blood

Animal blood (and in particular human blood) is an excellent example of a complex biofluid in which its physical properties are directly related to its physiological function.

We start this section with a brief description of blood composition and function for a better understanding. Later a rheological study of blood samples is done as an example of rheology applied to biological fluids.

5.1 Blood composition and function

Blood is a suspension of particles dispersed in an aqueous solution (called *plasma*). Plasma is formed principally by water and some organic and inorganic molecules like proteins, glucose or mineral oils and carbon dioxide. When it is isolated it behaves as a Newtonian fluid of viscosity 1.2 mPa· s. Dispersed particles can be divided in three different types: red blood cells (RBC), white blood cells (WBC) and platelets. RBC are the most relevant ones in the rheology of blood. WBC are in low concentration compared to RBC (which represents almost the 95%) and platelets are relatively small and can be neglected when studying the flow behavior.

RBC are disk-biconcave-shaped cells with a diameter of 7.2 μm and a thickness of 2.2 μm on the exterior and about 1 μm in the interior (fig. 11). RBC contain a big

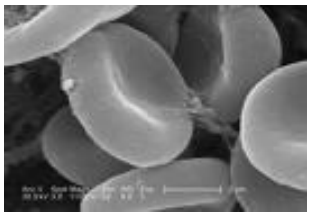

Figure 11: Red blood cells. Adapted from Daily Science

amount of hemoglobin which is capable of fixing the oxygen. RBC are then responsible for the transport of oxygen, and another gases, as well as nutrients and waste products of metabolism. Blood travels through veins, arteries and capillaries to reach all organs and tissues. A correct blood flow is of major importance for human's health.

5.2 Rheological properties

When blood is at rest cell aggregates called rouleaux tend to form (fig. 2 and 12). However, when a shear stress is applied blood flows and rouleaux start to decrease in size. The higher the shear stress, the smaller are the rouleaux, that eventually disappear and single RBC remain. That process implies a decrease of the viscosity of the fluid for an increasing applied shear rate: whole blood is shear-thinning (Chap. 2). It can be easily seen in fig. 12 where a sample of blood is at rest and under an applied shear rate of 500 s^{-1}.

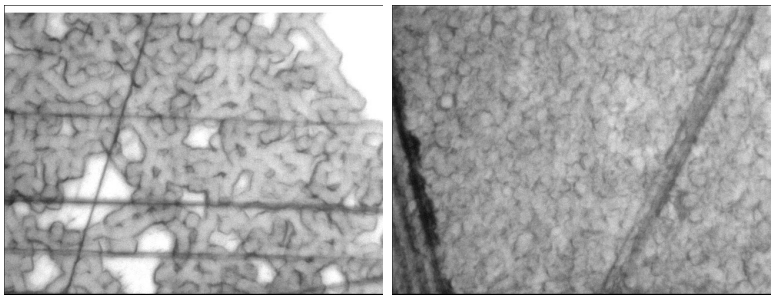

Figure 12: Blood samples under zero shear rate (left), and 500 s^{-1} (right). Courtesy of Roberto Steinbrüggen (Haake).

Rheological measurements can be done to probe such properties. But these measurements imply many experimental complexities that we cannot afford in our laboratory. In particular, the acquisition of fresh blood samples and a proper environment to keep them in good conditions, as well as an extremely sensitive rheometer that allows to do experiments in low shear regimes for low viscosity values. However, rheological experimental data of blood samples has been obtained for many specialized medical laboratories all over the world.

Relevant shear rates in blood circulatory system are in between 1 and 200 s^{-1}. For a similar range, shear thinning effects can be clearly seen in fig. 13 where viscosity values vary from 50 to 7 mPa·s approximately [12] (water's viscosity is 1 mPa·s).

Another rheological property which is crucial for blood function is its viscoelasticity. It is intrinsically related to BRC which have an important ability to deform. RBC's diameter is about 7 μm but they are able to deform in a thimble-like shape and pass through capillaries with smaller diameter of about 5 μm. They have the capacity to return to its original shape when they reach tubes of greater diameter (veins or arteries).

As we presented in Sec. 3.2. one of the simplest models describing viscoelastic fluids is the linear Maxwell model. And so it does for whole blood [13]. For times longer than its characteristic Maxwellian relaxation time blood is mainly viscous, and for times shorter than t_m elastic effects dominate.

All rheological properties are strongly dependent on the concentration of RBC, called hematocrit (H) (which is the volume fraction of RBC in blood). For this reason all experiments should be done at constant H.

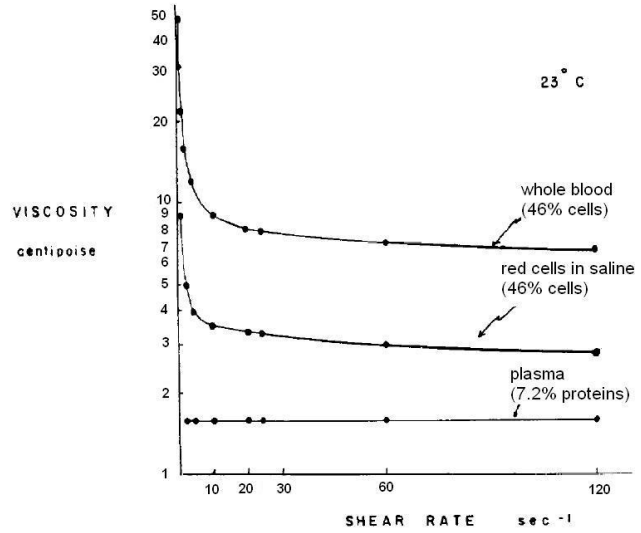

Figure 13: Viscosity versus applied shear rate for whole blood, red cells in saline, and plasma at $T = 23°$ C [12] (1 cP = 1 mPa·s).

5.3 Related diseases

It has been observed that anomalous values of blood viscosity can be correlated to many human diseases. Higher values of viscosity, due to an increase of hematocrit, have been related to cardiovascular events like ischaemia or stroke [14]. In a similar way, unusual viscosity profiles under applied shear rates can be associated to Diabetes and even to chronic anxiety states [11].

Consequently, a good knowledge of blood rheological properties can be helpful in detecting human diseases as well as designing suitable treatments.

6 Conclusions

A complete rheological characterization has been done for a micellar solution made of CPyCl-NaSal in water. It has been successfully proved that at low shear regimes it follows, as expected, the linear viscoelastic Maxwell model with a characteristic relaxation time of $t_m = 1.6$ s, which is in good agreement with the literature. In addition, an analysis of the non-linear region has been done. The obtained zero shear viscosity, as well as the shear-thinning behavior fit reasonably well with the expected values. First normal stress differences have also been measured in different shear rate regimes to prove that periodical oscillations appear. Finally, human blood has been studied as an example of rheology of a complex biofluid. Viscoelasticity and shear thinning effects have been illustrated, and anomalous values of its viscosity have been associated to different human diseases.

Aknowledgments

I would like to thank Roberto Steinbrüggen for making possible the measurements of normal forces with his rheometer. I also thank Ramon Planet for his help in my first experimental steps, and my advisor, Jordi Ortín, for introducing me in the subject of complex fluids, as well as for his special attention to this work and his valuable corrections.

References

[1] Gebhard Schramm, *A Practical Approach to Rheology and Rheometry*, Karlsruhe: Gebrueder HAAKE GmbH (2004).

[2] M. E. Cates, S. M. Fielding, *Rheology of giant micelles*, Advances in Physics **55**, 799 (2006).

[3] Ronald G. Larson, *The Structure and Rheology of Complex Fluids*, Oxford: Oxford University Press (1999).

[4] Tom A.Waigh, *Applied Biophysics. A molecular Approach for Physical Scientists*, Chichester: Wiley (2007).

[5] H. Rehage, H. Hoffmann, *Rheological Properties of Viscoelastic Surfactant Systems*, J. Phys. Chem. **92**, 4712 (1987).

[6] A. Méndez-Sánchez et al., *Instabilities of micellar systems under homogeneous and non-homogeneous flow conditions*, Rheol. Acta **42**, 56 (2003).

[7] M. Torralba, *Instabilities in Newtonian and non-Newtonian fluids*, PhD Thesis, University of Barcelona (2007).

[8] E. Guyon, J. P. Hulin, L. Petit, *Hydrodinamique physique*, Paris: InterEditions / CNRS Editions (1994).

[9] S. Manneville, *Recent experimental probes of shear banding*, Rheol. Acta **47**, 301 (2008).

[10] P. D. Olmsted, *Perspectives on shear banding in complex fluids*, Rheol. Acta **47**, 283 (2008).

[11] Jagan N. Mazumdar, *Biofluid Mechanics*, Singapore: Word Scientific (1992).

[12] R. Wells Jr., E. Merrill, H. Gabelnick, *Shear-Rate Dependence of Viscosity of Blood: Interaction of Red Cells and Plasma Proteins*, Transactions of the Society of Rheology **6**, 19 (1962).

[13] R. Collepardo Guevara, *Propuesta para aumentar el flujo sanguíneo en obstrucciones trombóticas y ateroscleróticas*, PhD Thesis, UNAM (2004).

[14] G.D.O. Lowe, A.J. Lee et al., *Blood viscosity and risk of cardiovascular events*, British Journal of Haematology **96**, 168 (1997).

Part II
Stochastic switches in the galactose signalling network

Abstract

Bistability is observed in many biological processes and in particular in processes involved in cellular differentiation. It can arise from positive feedback transcription networks and can be found in a colony of cells by the coexistence of two populations with different stable concentration of a specific protein. In [1], Yeast *Saccharomyces cerevisiae* cells were found to switch from one stable state to another one of the Galactose-signalling network. This network is mainly governed by a positive feedback loop and the switching rate depended on the state from which cells came. In order to describe such phenomena a deterministic model based on positive feedback loops is not sufficient. The aim of the present work is to understand from a theoretical point of view how these transitions are originated and predict the rate at which they jump between different stable states. For this purpose numerical simulations have been done based on Langevin equations with multiplicative noise and later compared to theoretical predictions derived from Fokker-Plank equations. In order to become familiar with the required numerical and theoretical techniques the Ginzburg-Landau model has been previously studied. Our results show that fluctuations in the maximal transcription rate can be responsible for this phenomenon. For the galactose network, our results predict that fluctuations in the levels of proteins Gal4p and Gal80 are crucial.

1 Introduction: Experimental evidence for transition rates in bistable systems

Bistability is present during cell differentiation and in many other biological processes like in cell-cycle regulation in Xenopus oocytes [2], or in lactose metabolism in *Escherichia coli* [3]. Bistability can be reached by different mechanisms but the most common is by means of feedback loops [5] where a component created as a result of a genetic pathway *feeds back* to a previous path stage modulating the rate production of an specific gene. In this work we will focus on an auto catalytic system where the product induces its own transcription rate (positive auto regulation). It has been shown, in vitro, that synthetic circuits with positive feedback in Yeast can lead to bistability [4], fig. 1.

In order to establish the dynamic evolution of any gene network, mathematical models can be developed. Deterministic and stochastic approaches can be done. Deterministic models based on time-dependent continuous descriptions with activation modelled by Hill functions can lead to monostable or bistable systems with two coexistant stable states. However, stochastic models taking into account fluctuations in the dynamics must be introduced to describe experimentally observed switches between those stable states.

In [1] the galactose-signalling network in Yeast *Saccharomyces cervesiae* was shown to exhibit bistability driven by a positive feedback loop mediated by protein Gal3p. In

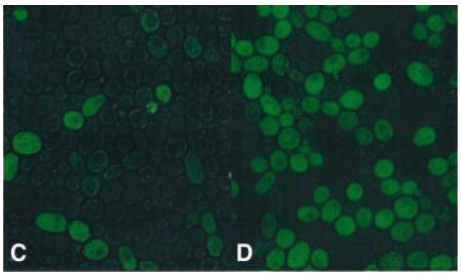

Figure 1: Population of *Sacharomyces cerevisiae* exhibiting bistability. Coexistent dark and bright stable states appear [4].

this particular network (fig. 2) the external signal input is the galactose, which passes through a 4-stage signalling cascade. Galactose enters the cell mediated by the Gal2p transporter. The intracellular galactose then binds to and activates the cytoplasmic signal transducer Gal3p. The activated Gal3p* binds to Gal80 in the cytoplasm reducing the corresponding concentration of Gal80 in the nucleus. Gal80 is an inhibitor of the transcription factor Gal4p, which activates the expression of genes GAL80, GAL3, GAL2, GAL1 (fig. 2). Thus, a decrease in the nuclear concentration of Gal80, increases the levels of Gal4p.

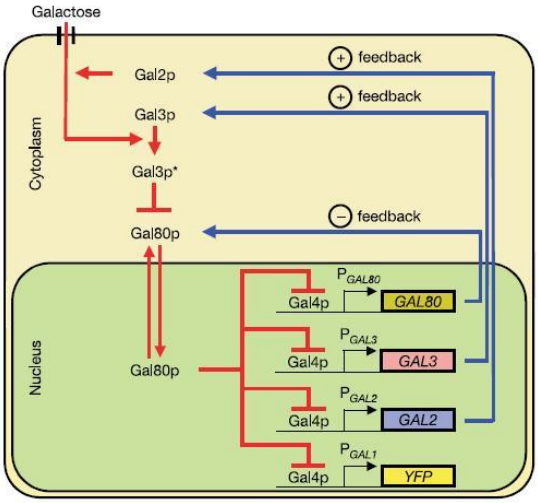

Figure 2: The galactose signalling pathway in Yeast *Saccharomyces cerevisiae* [1].

Both Gal2p and Gal3p enhance transcription activity, so they mediate two positive feedback loops. In the opposite way, Gal80 mediates a negative loop. However, it has been experimentally observed that the core loop controlling bistability is the positive feedback loop mediated by Gal3p [1]. The activity of Gal4p is experimentally observed by the expression of yellow fluorescent protein (YFP) which is linked to GAL1 promoter. Thus, fluorescence is used to observe, experimentally, bistability: a state defined by a

low activity of Gal4p, and dark appearene, (OFF state) coexists with another state of high activity, and bright appearence, (ON state). These states correspond to low and high concentration of Gal3p promoter, respectively, which is the variable we will mainly work with.

A useful analogy between the differential equation of the time evolution of the concentration of Gal3p and the equation of motion of an over damped particle in an energy landscape can be done to analyze stochasticity and stability of the expression states. This analogy will allow us to study the problem using a statistical mechanics approach (say Langevin and Fokker-Plank equations). In this analogy, the concentration is equivalent to the position of the particle and stable states correspond to minima of the energy landscape. To switch from one stable state to the other one the particle has to overcome an energy barrier, which is different if ON $\rightarrow$ OFF or OFF $\rightarrow$ ON transitions are considered. In addition, it has been experimentally observed [1], that for a given energy barrier the escape rates from ON states (ON $\rightarrow$ OFF transitions) are higher than those from OFF states (OFF $\rightarrow$ ON transitions). The aim of the present work is to develop a theoretical model that describes this observed switching behavior. A noise term associated to the maximal transcription rate will be applied. Due to the positive feedback loop, the noise intensity becomes different for each stable state (Chap. 2), being higher in the ON state.

This work will start with a wide description of stochasticity in bistable systems (Chap. 2). Later on, the analysis of a well-known dynamics based on the symmetric Ginzburg-Landau potential (Chap. 3) will be done. After a good comprehension of how this model works, the same methodology and techniques will be applied to the stochastic positive feedback model (Chap. 4).

2 Stochasticity in bistable systems

Bistable systems are systems with two stable states each of them corresponding to a minimum of energy and separated by an energy barrier. In deterministic situations, the system, starting at any point, would evolve toward a local minimum of energy and remain there indefinitely if no perturbation were applied. For zero-dimensional systems the dynamical behavior is governed by the following differential equation [6]:

$$\frac{\partial x}{\partial t} = -\frac{\partial V}{\partial x} \tag{1}$$

where $V(x)$ is the energy potential and x the system's variable. According to this scheme, transitions from one minimum to the other one would not be allowed. But, in fact, our main interest is related to these transitions. For that reason we will deal with a stochastic description based on the Langevin and Fokker-Plank equations.

2.1 Langevin and Fokker-Plank equations

The Langevin equation (Eq. 2) takes into account a random source of fluctuations that allows the particle to escape from minima and switch between stable states.

$$\frac{\partial x}{dt} = f(x) + g(x)\eta \,. \tag{2}$$

The driving force associated to the potential is $f(x) = -\frac{\partial V}{\partial x}$ and η is a random term accounting for the system's noise. We will use a gaussianly distributed noise with zero mean value, uncorrelated in time and with intensity ε:

$$\langle \eta(t) \rangle = 0 \,, \tag{3}$$

$$\left\langle \eta(t)\eta(t') \right\rangle = 2\varepsilon\delta(t-t') \,. \tag{4}$$

Depending on the function $g(x)$ in Eq. 2 we will talk about, additive noise if $g(x)$ is a constant (e.g. $g(x) = 1$) or multiplicative if $g(x)$ is a function of x.

Due to the random term, $x(t)$ is no more a deterministic variable but a stochastic one. This makes us work with its probability distribution $P(x,t)$ and not with the variable itself. The dynamic equation of the system will be described by its Fokker-Plank equation

$$\frac{\partial P}{\partial t} = -\frac{\partial}{\partial x} f(x)P(x,t) + \varepsilon \frac{\partial}{\partial x} g(x) \frac{\partial}{\partial x} g(x)P(x,t) \,, \tag{5}$$

with stationary probability [6]:

$$P_{st} = N \exp\left\{ \int \frac{f(x) - \varepsilon g(x) g'(x)}{\varepsilon g(x)^2} \right\} \,. \tag{6}$$

For additive noise ($g(x) = 1$), P_{st} has the same form as the Boltzmann equilibrium distribution with a potential $V(x)$,

$$P_{st} = N \exp\left\{ -\frac{V(x)}{\varepsilon} \right\} \tag{7}$$

where N is the normalization factor. It is important to realise that the maxima of this distribution, $\bar{x}$, do correspond with the mimina, x_{min}, of the deterministic potential $V(x)$. For $\varepsilon = 0$ we would recover the deterministic result and the stationary probability would be zero everywhere except in the minima of energy:

$$P_{st} = N\delta(x - x_{min}) \,. \tag{8}$$

As we increase ε the probability distribution gets wider. So, additive noise does not change the position of stable states but lets the particle overcome the energy barrier.

For multiplicative noise, an effective potential, V_{eff}, can be defined in order to rewrite P_{st} using the Boltzmann equilibrium distribution:

$$P_{st} = N \exp\left\{ -\frac{V_{eff}(x)}{\varepsilon} \right\} , \tag{9}$$

where

$$V_{eff}(x) = \int -\frac{f(x) - \varepsilon g(x) g'(x)}{g(x)^2} \, . \tag{10}$$

It is worth stressing that the extrema $\bar{x}$ of the resulting stationary probability coincide with the minima of the effective potential but not with those of the deterministic potential.

2.2 Transition rates

A particle, initially placed at one stable state, has a certain probability to escape from its potential well, and after a certain time T (which is called the Arrhenius, Kramers, or herein transition time) it can reach the other stable state. For an additive noise its analytical expression is given by [8, 9, 10]:

$$T(x_1 \to x_2) = \frac{2\pi}{\sqrt{|V''(x_1)V''(b)|}} \exp\left(\frac{V(b) - V(x_1)}{\varepsilon}\right) \, , \tag{11}$$

where V'' denotes the second derivative of the potential, x_1 and x_2 refer to both stable states and b to the position of the energy barrier. ε is the intensity of the additive noise. As expected, for small ε, the Arrhenius time will be longer than for huge ε values.

The transition rates found experimentally for the galactose network [1] for different energy barriers follow a behavior similar to transition rates driven by additive noise. Accordingly, and in order to analyze the observed behavior in the galactose-signalling network, we will test wheter multiplicative noises that are constant all around each minima and just vary on the enrgy barrier (fig.3) elicit transition rates that can be characterized in terms of Eq. 11. Thus, for a dynamics with multiplicative noise $g(x)$,

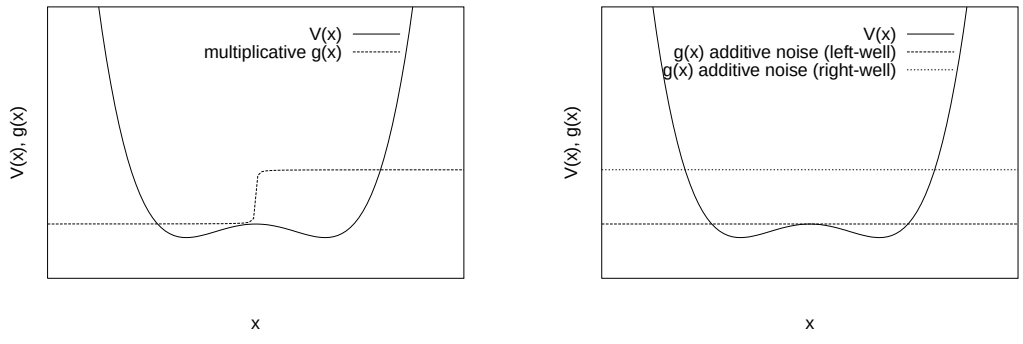

Figure 3: Ginzburg-Landau potential and $g(x)$ noise function for multiplicative (left) and additive (right) noise dynamics. Gaussian noise is described by eq. 3, 4. Right: Two different constant functions are plotted, each of them corresponding to the value of the function $g(x)$ (plotted in the left panel) on each minima of the potential ($g(x) = g(x_1)$, and $g(x) = g(x_2)$).

with $g(x)$ such as the one shown in fig. 3 (left panel), we will test whether the transition rate follows:

$$T(x_1 \to x_2) = \frac{2\pi}{\sqrt{|V''(x_1)V''(b)|}} \exp\left(\frac{V(b) - V(x_1)}{\varepsilon g(x_1)^2}\right) , \tag{12}$$

that corresponds to a dynamics in a potential $V(x)$ with additive noise of intensity $\varepsilon g(x_1)^2$ (fig.3, left panel). This can be computed analogously for $\mathrm{T}(x_2 \to x_1)$. In the next section we test whether this hypothesis is valid using the Ginzburg-Landau model. Afterwards we apply it to a model for positive feedback.

In this scheme, the only inconvenience may arise from the fact that the minima obtained from an additive or multiplicative noise dynamics are not equal. However, these differences are very small for the particular examples we are interested in and can be neglected.

2.3 Numerical simulations of stochastic processes

We will base the study of the dynamical behavior of our system on the trajectory of many particles placed on a suitable potential landscape. Stochastic trajectories will be generated numerically, using the Heun algorithm [6, 11], over a period of time T. A later statistical analysis of these trajectories will allow to obtain the P_{st} and calculate the transition rates between stable states.

The Arrhenius time will be calculated as the average time that each particle remains in a potential well: since the particle enters the potential well until it leaves (we consider that the particle enters/leaves the well when it passes through the middle point between a minimum and the maximum of energy). We check that, eventually, the particle overcomes the energy barrier and reaches the other stable state. Sampling averages are computed over the whole set of simulated particles. The transition rate is expressed as the inverse of the transition time.

3 Stochastic symmetric bistable systems

We start by studying a well-known system with symmetric bistable potential landscape, in order to get used to theoretical and numerical techniques. We will use the Ginzburg-Landau potential [12] for this purpose. The Ginzburg-Landau potential, when no external forces are applied is given by:

$$V(x) = -a\,\frac{x^2}{2} + b\,\frac{x^4}{4} . \tag{13}$$

We take $b = 1$ for simplicity. For values of $a > 0$, $V(x)$ has two minima, $x = \pm\sqrt{a}$, which correspond to both stable states, and a maximum placed at $x = 0$ for any value of a. The energy barrier depends on a values, too (fig. 4).

Thus, in this system both stable states have the same energy value, and the same energy barrier has to be overcome to switch to the other state. The Arrhenius time and the transition rates should then be, equivalent for both states.

We will start checking that our model works properly for an additive noise dynamics. Afterwards, following the assumption we did in Sec. 2.2 we will consider a multiplicative

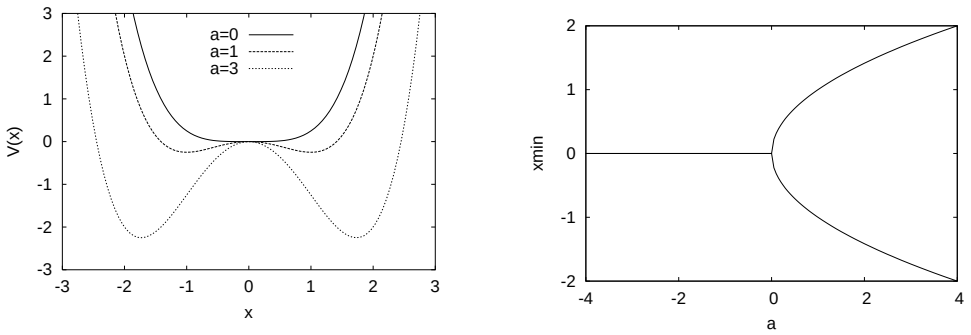

Figure 4: Left: Ginzburg-Landau potential for different a values. Right: Theoretical bifurcation diagram for the Ginzburg-Landau potential. Stable states (one or two) ar plotted for different a values.

noise dynamics, which we expect will give us an asymmetric switching rate behavior that is characterized in each case by the transition rates of additive noise dynamics.

3.1 Additive noise. Numerical results

The Langevin equation (Eq. 2) for an additive noise based dynamics, and its stationary probability distribution P_{st} (Eq. 7) are given by:

$$\frac{\partial x}{dt} = ax - x^3 + \eta \;\; ; \;\; P_{st} = N \exp\left\{ \frac{a\frac{x^2}{2} - \frac{x^4}{4}}{\varepsilon} \right\} , \tag{14}$$

and the noise intensity is the same we described in Eq. 4. The P_{st} can be reproduced

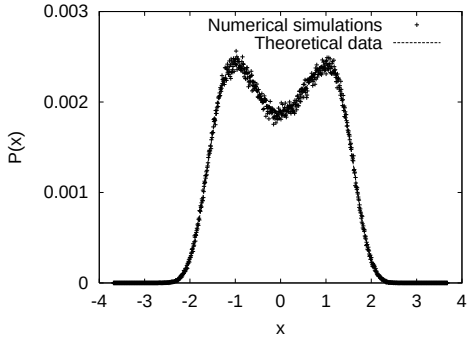

Figure 5: Comparison of the numerically obtained P_{st} with the theoretical plot (Eq. 14), for a Ginzburg-Landau potential with constant $a = 1$, $\varepsilon = 1$. Numerical parameter values: Integration time step = 0.01; Number of iterations = 100.000; Number of particles = 1.

numerically using the Heun algorithm (fig. 5). The obtained distribution is symmetric,

and its minima (located at $x = \pm 1$) do coincide, as expected, with the minima of the deterministic potential (for $a = 1$).

We are mainly interested in calculating, numerically, the transition time between both stable states, using the numerical tools specified in Sec. 2.3. Numerical results are compared to the theoretical curve in Eq. 12. A good agreement between both curves is obtained (fig. 6), and the logarithm of the transition time versus the inverse of the noise intensity, ε, as well as versus the energy barrier, ΔU, obeys a linear relation. Similar results have been obtained for both symmetric stable states but they are plotted together for a better statistical treatment.

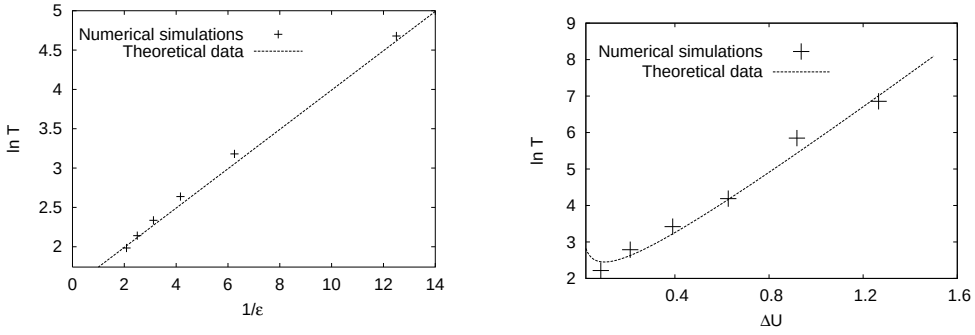

Figure 6: Left: Numerical simulations and theoretical curve (Eq. 11) for the logarithm of the transition time versus the invers of the noise intensity for a Ginzburg-Landau potential of constant $a = 1$ and $\Delta U = 0.25$. Right: Numerical simulations and theoretical curve (Eq. 11) for the logarithm of the transition time versus the energy barrier for a Ginzburg-Landau potential with $\varepsilon = 0.2$. Numerical parameter values: Integration time step = 0.01; Number of iterations = 100.000; Number of particles $n = 20$.

3.2 Multiplicative noise. Numerical results

We can now proceed to apply a multiplicative noise dynamics on the Ginzburg-Landau model. We will use a multiplicative function $g(x)$ that remains constant all around both minima (x_1 and x_2) and variable on the energy barrier (fig. 3). Although this functions has no biological sense in this specific model, it will have a crucial interest when we deal with the stochastic positive model in Chap. 4 because a similar function will be able to reproduce the observed switching behavior observed in the galactose-signalling network [1].

The multiplicative function we use is given by,

$$g(x) = \frac{1}{\pi}(\arctan 8\, x + \frac{\pi}{2}) + 1 \tag{15}$$

which takes $g(x) \approx 1$ around x_1 and $g(x) \approx 2$ around x_2 and is derivable for all x range. Its stationary probability distribution and bifurcation diagram are illustrated in fig. 7. Although the Ginzburg-Landau deterministic potential is symmetric, the asymmetrical

applied noise will turn it into an asymmetric P_{st} (fig. 7). The x_1, with a lower intensity noise value, has a higher stationary probability, as expected. The location of stable states slightly changes from the deterministic ones, but for the range of values of a we are interested in, the differences are small enough to be neglected.

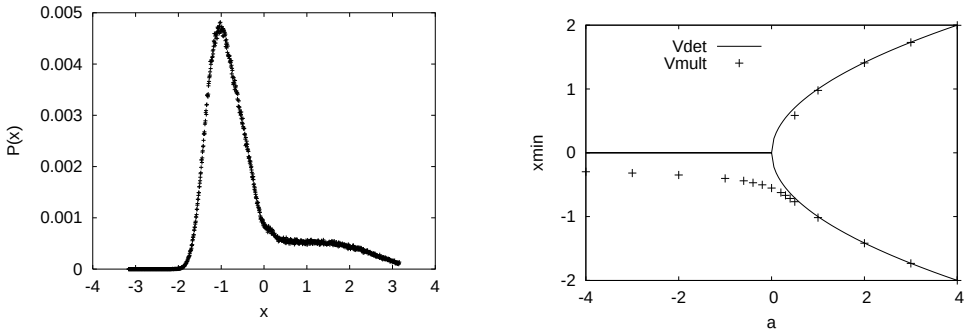

Figure 7: Left: Numerically obtained stationary probability distribution for a Ginzburg-Landau potential with multiplicative noise (Eq. 15), $a = 1$, $\varepsilon = 1$. Numerical parameter values as in Fig. 5. Right: Theoretical bifurcation diagram for both the deterministic and multiplicative Ginzburg-Landau potentials ($\varepsilon = 1$).

In addition, we will consider two more multiplicative functions which are strongly shifted, one to the right ($g_1(x)$) and the other one to the left ($g_2(x)$), see fig. 8, Eq. 16.

$$g_1(x) = \frac{1}{\pi}(\arctan 8 \cdot (x - 100) + \frac{\pi}{2}) + 1\,, \quad g_2(x) = \frac{1}{\pi}(\arctan 8 \cdot (x + 100) + \frac{\pi}{2}) + 1\,. \quad (16)$$

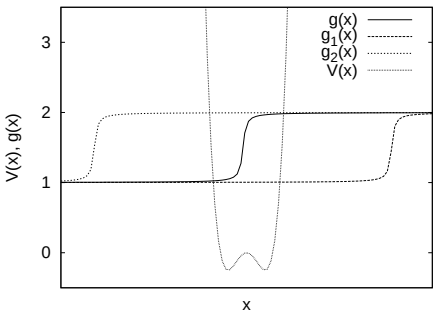

Figure 8: Qualitative representation of multiplicative functions: *normal* $g(x)$, Eq. 15, right-shifted $g_1(x)$, left-shifted $g_2(x)$, Eq. 16, and Ginzburg-Landau potential.

For these functions the transition rates should follow Eq. 12 and should be symmetric ($T(x_1 \to x_2) = T(x_2 \to x_1)$), as we find indeed (fig. 9, left panel). When the right-shifted multiplicative function $g_1(x)$, with $g_1(x_1) = g_1(x_2) \approx 1$ (low noise) is used, the

numerically obtained transition rates fit correctly the theoretical curve corresponding to additive noise dynamics, Eq. 12. And in a similar way for $g_2(x)$ (high noise), with $g_2(x_1) = g_2(x_2) \approx 2$.

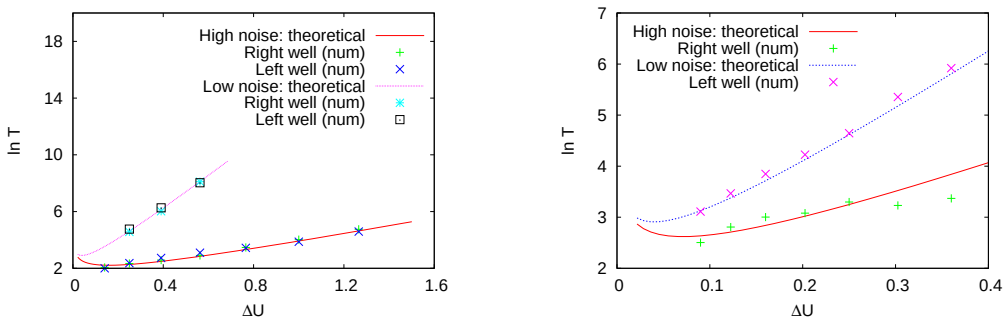

Figure 9: Logarithm of the transition time versus the invers of the noise intensity for a Ginzburg-Landau potential with multiplicative noise. Left: Right and left shifted, $g_1(x)$ and $g_2(x)$, functions have been used (Eq. 16). Theoretical curves are calculated from Eq. 12 with $g_1(x_1) = g_1(x_2) \approx 1$, $g_2(x_1) = g_2(x_2) \approx 2$, and $\varepsilon = 0.08$. Right: $g(x) = \frac{1}{3\pi}(\arctan 8\, x + \frac{\pi}{2}) + 1$ multiplicative function has been used, $g_1(x_1) \approx 1$, $g_2(x_2) \approx 1.33$, $\varepsilon = 0.08$. Numerical parameter values as in Fig. 6.

When a multiplicative function with $g_1(x_1) \neq g_2(x_2)$ as in Eq. 15 is used, we expect asymmetric transition rates. The obtained numerical simulations for both stable states are shown in fig. 9, right panel. Again, we get a good agreement between numerical results and the theoretical curves (Eq. 12). As expected, different behaviors are observed for right (x_2) and left (x_1) states: much higher transition time values are associated to the x_1, which has lower noise intensity. In addition, the transition rate for each state fits properly with the corresponding theoretical additive curve (Eq. 12).

In summary, we have been able to correctly compute the transition rates and have found that multiplicative noise dynamics with nearly constant values of noise on the stable states exhibit transition rates that can be described by Eq. 12. This let us turn to the *true* biological model, based on a positive feedback network.

4 Stochastic positive feedback model

We have finally reached the last step of our work: develop a theoretical model based on a positive feedback dynamics that can reproduce the observed switching behavior in the gallactose-signalling network [1], using all the theoretical and numerical techniques we have been testing.

4.1 Deterministic behavior

First of all, we have to define the deterministic differential equation which characterizes the transcription network. We will work with the usual description of positive feedback loops based on Hill functions [5, 7]. Specially, we will take the same deterministic

equation as in [4], to study bistability driven by synthetic positive feedback in yeast cells.

We will reduce our genetic network to the core positive feedback loop controlled by Gal3p, to reduce the system's complexity and better understand the underlying biological behavior. Thus, we propose the differential equation of the time evolution of the concentration of Gal3p to be:

$$\frac{\partial x}{\partial t} = \frac{s \cdot x^n}{a^n + x^n} + r - kx \, . \tag{17}$$

The first term on the right hand-side of Eq. 17, based on the Hill function, describes the positive loop mediated by Gal3p, where x is the concentration of *Gal3p* (and for this reason it must remain $x \geq 0$). The constant parameter s is the maximal synthesis rate of activator, and it is strongly related to the concentration of the transcription factor Gal4p and the inhibitor Gal80. n is the cooperativity of activation and a^n is the dissociation constant of the activator from its DNA binding site. The second term, r, describes the basal rate of synthesis of Gal3p, and the third one, its degradation rate.

With this dynamical equation, whether monostable or bistable dynamics can arise depending on the value of each kinetic parameter (we see it graphically in fig. 10 where Eq. 17 has been separated in two curves and stable states appear as their intersecting points). In order to guarantee bistability, and following the same criteria used in [4], we will choose these parameters to be: $4 \leq s \leq 148$ min^{-1}, $n = 3$, $r = 0.1$ min^{-1} and $k = 1$ min^{-1} (concentrations and concentration-based parameters are taken to be non-dimensional). In order to simplify the problem we will keep constant all kinetic parameters except s.

Integrating the differential equation (Eq. 17) we find the corresponding energy potential:

$$V(x) = -\int f(x) = -(s+r)\cdot x + \frac{kx^2}{2} + s \cdot a \left(\frac{1}{6} \ln \frac{(a+x)^2}{a^2 - ax + x^2} + \frac{1}{\sqrt{3}} \arctan \frac{2x-a}{a\sqrt{3}} \right) . \tag{18}$$

This potential is not symmetric. The position of both stable states x_1 and x_2, which correspond to OFF (dark) and ON (bright) states and its maximum depends on the s value. Nevertheless, x_1 always remains close to $x_1 \approx 0$, and $x_2 \approx s$. In addition, for all the s range we are working with $V(x_2) < V(x_1)$ and the energy barrier will thus be different between both stable states (fig. 10).

But this deterministic equation do not account for transition rates between stable states and a stochastic term must be added in Eq. 17 in order to include them in our model.

4.2 Multiplicative noise. Numerical results

We will use a very similar multiplicative function as the $g(x)$ we introduced in the Ginzburg-Landau model:

$$g(x) = \frac{x^n}{a^n + x^n} \, . \tag{19}$$

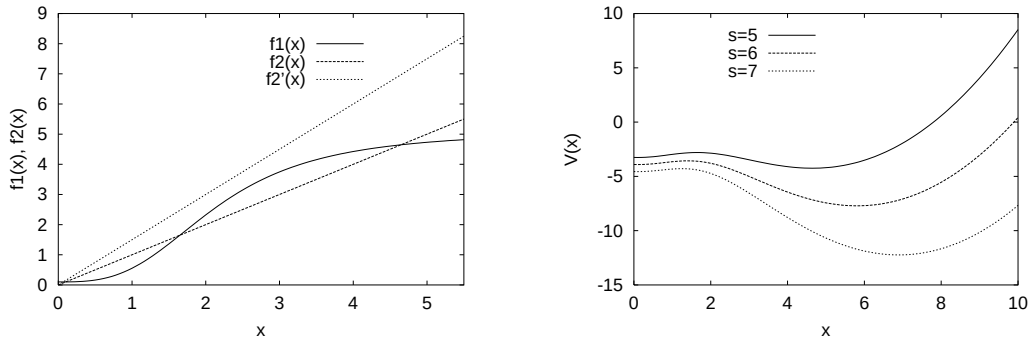

Figure 10: Left: Monostable and bistable regimes, for two different k values ($k = 1$ min^{-1}, $k' = 1.5$ min^{-1}, $s = 5$ min^{-1}, $n = 3$, $r = 0.1$ min^{-1}): $f1(x) = \frac{s \cdot x^n}{d+x^n} + r$, $f2(x) = kx$. Intersection points correspond to stable states. Right: Energy potential of the deterministic positive feedback model, for diferent s values: $s = 5\,, 6\,, 7$ min^{-1}, $k = 1$ min^{-1}.

Its value is constant around both stable states ($g(x_1) \approx 0$, $g(x_2) \approx 1$). In addition, $g(x = 0) = 0$, which prevents the particle to go to negative values (x is a concentration variable and must remain positive). The corresponding Langevin equation is:

$$\frac{\partial x}{\partial t} = (s + \eta)\frac{x^n}{a^n + x^n} + r - kx\,, \tag{20}$$

The crucial idea of this $g(x)$ arises from the fact that it can be identified as a noise term associated to the transcription rate s. Consequently, our hypothesis is that an external noise that is related to fluctuations in the concentration values of Gal4p and Gal80 is responsible for the observed swithcing rates in [1]. The resulting effective potential

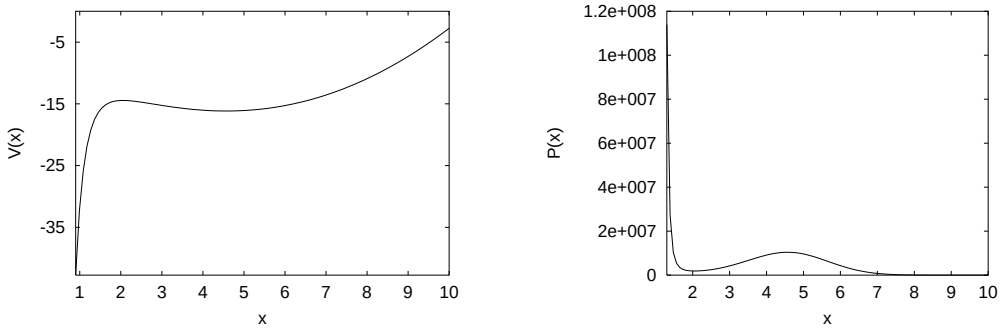

Figure 11: Left: Effective potential for the positive feedback model. Right: Non-normalized theoretical stationary probability P_{st} derived from V_{eff} for the positive feedback model. The used multiplicative function is given by Eq.19 where $g(x_1) \approx 0$, $g(x_2) \approx 1$; $\varepsilon = 1$.

and stationary probability distribution for these dynamical equations are represented in fig. 11. It is important to remark that the relative stability of both minima has been exchanged from its deterministic position (fig. 10): x_1 has now much lower energy values than x_2 (and consequently, much higher P_{st} values). In addition, the region of bistability becomes slightly narrower, and the position of x_1 and x_2, quite shifted (fig. 12). Again, these differences will be very small in the s range we are interested in and we will neglect them. With this dynamical equation we proceed to calculate the transition time between

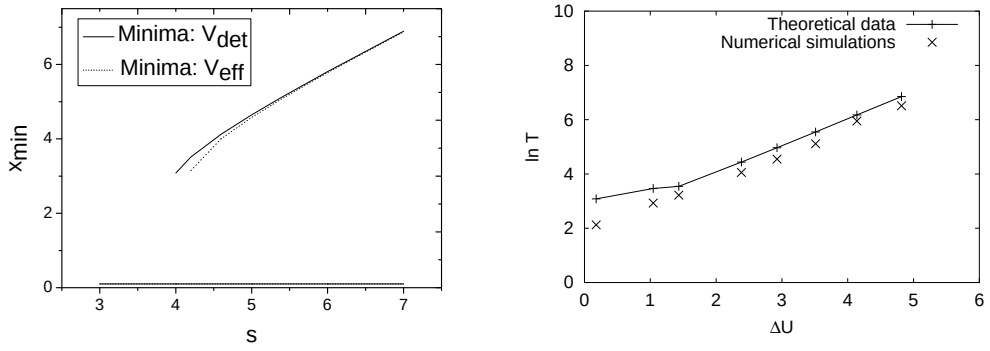

Figure 12: Left: Bifurcation diagram for the positive feedback potential (deterministic V_{det} and the effective V_{eff} derived from a multiplicative noise dynamics, Eq. 19, $\varepsilon = 1$). Right: Numerical simulations of the logarithm of the transition time versus the energy barrier of the positive feedback deterministic potential, using the shifted multiplicative function $g_1(x)$ with $g_1(x_1) = g_1(x_2) \approx 1$; $\varepsilon = 1$. Numerical simulations are compared to the theoretical curve (Eq. 12). Numerical parameter values as in fig. 6.

both stable states. As we did for the Ginzburg-Landau potential, we start with a previous analysis, using a shifted multiplicative function $g_1(x) = (x - 100)^n/(a^n + (x - 100)^n)$. This analysis will only be valid for the x_2 state. Otherwise, considering a non-zero noise all around x_1 we would come to x negative values. A good agreement between numerical simulations and theoretical data, based on an additive noise dynamics is obtained, Eq. 12, (fig. 12, right panel). However, simulations with a higher number of events, would permit a better statistical treatment, and probably, a better agreement. We can finally use the *real* $g(x)$ function (Eq. 19).

Plotting the logarithm of the transition rate (the inverse of the transition time) of our numerical simulations versus the deterministic potential, we see that they are in fair agreement with the theoretical prediction, Eq. 12, (fig 14, left panel).

Unfortunately, we will only be able to reproduce the multiplicative dynamics on the right potential well (it means $x_2 \to x_1$, $ON \to OFF$ transitions). The noise intensity on the left well is nearly zero and the theoretically predicted value of its transition time ($x_1 \to x_2$, or $OFF \to ON$) is extremely large. Numerically, we will not be able to calculate it either. So, we place the particle initially at x_2 and we compute the time that it takes to overcome the energy barrier and reach x_1. There, the particle will not be able to overcome the energy barrier again, and will remain on x_1 *forever*. An example of one particle's trajectory is shown in fig. 13. The $x_1 \to x_2$ transitions, although they

can not be included in fig. 14, should appear in the lower-left part, that corresponds to small energy barriers and very low transition rates.

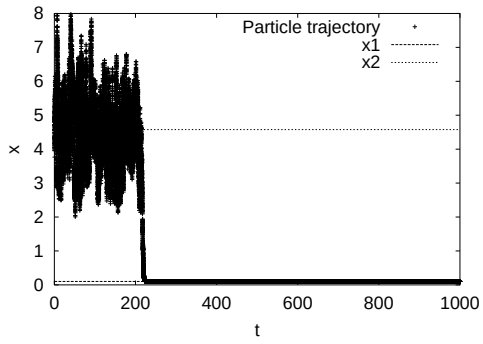

Figure 13: Paricle's trajectory for a multiplicative noise dynamics (g(x) given by Eq. 19; $\varepsilon = 1$). $x1$ and $x2$ refer to both stable states. The particle, initially placed at x2 position, oscillates and after a while reaches the x1 postition to remain there. Numerical parameter values: Integration time step = 0.01; Number of iterations = 100.000; Number of particles = 1.

This final plot has to be compared to experimental data obtained by van Oudenaarden in 2005 [1] in a population of yeast *Sacharomyces cerevisiae* (fig. 14). They saw

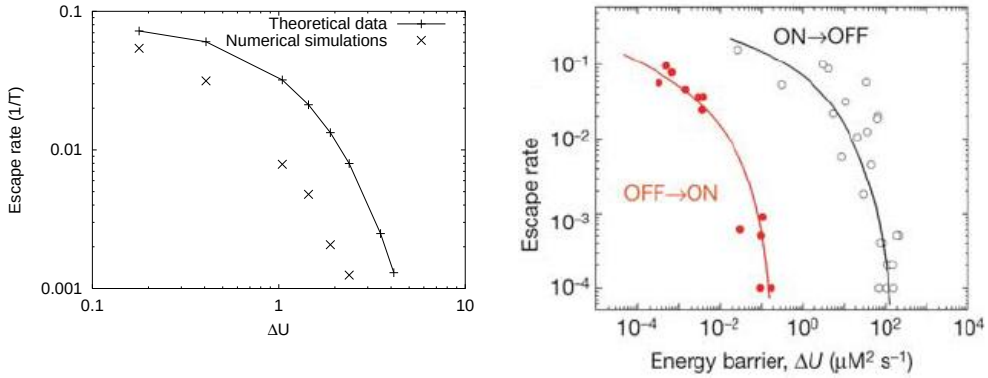

Figure 14: Left: Numerical transition rates for $x_2 \to x_1$ transitions versus the energy barrier, ΔU (multiplicative function (Eq. 19) with $g(x_1) \approx 0$, $g(x_2) \approx 1$; $\varepsilon = 1$). Numerical parameter values as in fig. 6. Right: Experimentally measured escape rates as a function of the calculated energy barriers [1]

experimentally, that the transition rates for $ON \to OFF$ switches ($x_2 \to x_1$ in our system) were higher than the $OFF \to ON$ ones ($x_1 \to x_2$), and it is exactly the same qualitative behavior we have predicted theoretically, and numerically obtained. In addition, they observed that the fluctuations in Gal3p expression (the variable x), where larger in the ON state (x_2) than in the OFF one (x_1), which do coincide, again, with

our numerical simulations (an example can be seen in fig. 13). Differences between numerical simulations and theory prediction may be due to a not enough accurate multiplicative function. Using an step-like function, with really constant values all around each minima, we may reduce these differences.

The overall behavior may seem anti intuitive: given an energy barrier, the escape rates from the ON state are larger than escape rates from the OFF one. For internal noise dynamics it should have no physical sense. However, considering an external multiplicative noise, with different noise values for every stable state we could generate such behavior. Or, it would be equivalent to say that the multiplicative dynamics changes the stability of the stable states in such a way that the energy barrier that have to overcome the particles coming from the OFF and ON states is no longer the same, but the energy barrier for $OFF \rightarrow ON$ transitions is much higher (and the transition rates much lower).

5 Conclusions and future perspectives

A theoretical stochastic model based on a positive feedback network has been developed in order to describe the experimentally observed switching behavior on Galactose-signaling network of yeast *Sacharomyces cerevisiae* cells [1]. This system exhibited bistability on the concentration of the protein Gal3p (rapported by the fluorescent protein YFP) which was translated on the coexistence of a dark and a bright cell subpopulations. In addition, switches between both stable states were observed, with a different scape rate depending on the sate of origin ($ON \rightarrow OFF$ transitions are much frequent than $OFF \rightarrow ON$ transitions).

In order to understand this behavior we have developed a model based on a multiplicative noise dynamics, given by a multiplicative function with higher noise intensity on the ON state, and lower on the OFF state. The noise term has been associated to the feedback transcription rate, which is directly related to the concentration of the transcription factor Gal4p and the Gal80 protein. Consequently, fluctuations on both concentrations might be seen as the initial inducer of the observed switching behavior.

In this project, different theoretical approaches and numerical techniques have been initially applied to a symmetric stochastic model based on the Ginzburg-Landau potential, to verify that they run correctly. Later simulations on the stochastic positive feedback model have been performed. The obtained results show the same qualitative behavior as we expected. In addition, larger fluctuations have been obtained for the ON state of the Gal3p expression, which is, again, in good agreement with experimental evidences. However, differences on the escape rate values for the transitions in both directions (OFF→ON, ON→OFF) are much higher that the experimental results.

The addition of an internal noise may be a possible way to reduce these differences [13]. The internal noise, inherent to the concentration of Gal3p, would be translated to an increase of the noise intensity of both stable states, but would have a major influence on the OFF state (which initially had a very low noise value, $g(x_1) \approx 0$). This may turn to higher escape rates of OFF→ON transitions, and smaller differences between switches in both directions.

Aknowledgments

I would like to thank my mother for her unconditional patience and CMREB for their ability to make life happier. I also thank Bruno Juliá for the support he has offered, and specially my advisor, Marta Ibañes, for her constant motivation and dedication on the project.

References

[1] M. Acar, A. Becskei, A. van Oudenaarden, *Enhancement of cellular memory by reducing stochastic transitions*, Letters to nature **435**, 228 (2005).

[2] J. Ferrell Jr, E. Machleder, *The Biochemical Basis of an All-or-None Cell Fate Switch in Xenopus Oocytes*, Science **280**, 895 (1998).

[3] J. Vilar , C. C. Cuet, S. Leiber, *Modeling network dynamics: the lac operon, a case study*, Journal of Cell Biology **161**, 471 (2008).

[4] A. Becskei, B. Séraphin, L. Serrano, *Positive feedback in eukaryotic gene networks: cell differentiation by graded to binary response conversion*, The EMBO Journal **20**, 2528 (2001).

[5] U. Alon, *An Introduction to Systems Biology. Design Principles of Biological Circuits*, NW: Chapman & Hall / CRC (2007).

[6] J. García-Ojalvo, J.M. Sancho, *Noise in Spatially Extended Systems*, New York: Springer-Verlag (1999).

[7] J. D. Murray, Mathematical biology Vol. 1, New York: Springer (2003).

[8] J. M. Sancho, *Notes of the Fokker-Planck Equation*, Barcelona.

[9] W. Horsthemke, R. Lefever, *Noise-Induced Transitions*, Berlin: Springer-Verlag (1984).

[10] N. G. van Kampen, *Stochastic processes in physics and chemistry*, Amsterdam: North-Holland (1992).

[11] M. San Miguel, R. Toral, *Stochastic effects in Physical Systems*, Cond-Mat/9707147 (1997).

[12] R. K. Pathria, *Statistical Mechanics*, Oxford: Butterworth-Heinemann, 2nd ed.(1996).

[13] W. Bialek, *Stability and noise in biochemical switches*, Cond-Mat/0005235 (2000).